Leraillez, Akseli; St-Pierre, Luc

Fracture toughness of hierarchical lattice materials

Published in:
International Journal of Solids and Structures

DOI:
10.1016/j.ijsolstr.2025.113374

Published: 15/06/2025

Document Version
Publisher's PDF, also known as Version of record

International Journal of Solids and Structures 316 (2025) 113374

Contents lists available at ScienceDirect

International Journal of Solids and Structures

journal homepage: www.elsevier.com/locate/ijsolstr

Fracture toughness of hierarchical lattice materials

Akseli Leraillez, Luc St-Pierre *

Aalto University, Department of Mechanical Engineering, PO box 14200, 00076 AALTO, Finland

ARTICLE INFO

Keywords:
Lattice material
Hierarchy
Honeycomb
Fracture toughness
Finite Element simulation

ABSTRACT

Natural materials, such as wood and bone, have a high fracture toughness and this is often attributed to their hierarchical microstructures. While previous studies have shown that hierarchy can increase the buckling strength of lattice materials, a detailed analysis of its impact on fracture toughness is missing. Here, we used analytical modeling and finite element simulations to predict the mode I and mode II fracture toughness of three hierarchical topologies: hexagonal, triangular, and Kagome lattices. Hierarchy significantly improved the fracture toughness of the bending-dominated hexagonal lattice. Notably, the hierarchical hexagonal lattice has a fracture toughness K_{IC} that scales linearly with relative density $\bar{\rho}$, whereas its non-hierarchical counterpart has $K_{IC} \propto \bar{\rho}^2$. In contrast, hierarchy did not improve the toughness of stretching-dominated triangular and Kagome lattices. Hierarchy did, however, modify the behavior of a Kagome lattice: its hierarchical design has a toughness that scales linearly with relative density, whereas $K_{IC} \propto \sqrt{\bar{\rho}}$ for its non-hierarchical counterpart. This work presents scaling laws for the fracture toughness of hierarchical lattices, enabling the design of tough architectures at very low densities.

1. Introduction

Lattices materials are periodic cellular solids generated by tessellating a unit cell in 2D or 3D (Fleck et al., 2010). Lattice materials allow for a wide range of mechanical properties and are often used in lightweight applications, such as aircraft fuselages (Kostopoulos and Vlachos, 2017). The strength and stiffness of lattice materials are, however, limited by theoretical upper bounds, and several topologies approaching these limits have already been identified (Berger et al., 2017; Hsieh et al., 2019; Tancogne-Dejean et al., 2018). In contrast, the fracture toughness of lattices is theoretically unbounded, which leaves room for further improvements.

The relationship between the architecture of a lattice and its fracture toughness has been investigated analytically, numerically, and experimentally (Berkache et al., 2022; Fleck and Qiu, 2007; Gu et al., 2018; Lipperman et al., 2007; Luan et al., 2022; Maiti et al., 1984; Omidi and St-Pierre, 2023a,b; Romijn and Fleck, 2007; Seiler et al., 2019; Tankasala et al., 2015). These studies have shown that the fracture toughness of an elastic-brittle lattice can be expressed in non-dimensional form as:

$$\frac{K_{IC}}{\sigma_{ts}\sqrt{L}} = D_I \bar{\rho}^d \quad \text{and} \quad \frac{K_{IIC}}{\sigma_{ts}\sqrt{L}} = D_{II} \bar{\rho}^d, \tag{1}$$

where K_{IC} and K_{IIC} are the fracture toughness under modes I and II, respectively; σ_{ts} is the tensile strength of the constitutive material; L is the length of the struts; $\bar{\rho}$ is the relative density; whereas D_I, D_{II}, and d are topology specific constants given in Table 1 for hexagonal, triangular, and Kagome lattices. The exponent d has a strong effect on fracture toughness. Bending-dominated topologies, such as a hexagonal lattice, have an exponent $d = 2$ and consequently, a low toughness. Stretching-dominated architectures, such as a triangular lattice, are significantly tougher, with a fracture toughness that scales linearly with relative density ($d = 1$). Surprisingly, some stretching-dominated topologies, like the Kagome lattice, exhibit a crack tip blunting phenomenon, which leads to $d = 0.5$ and results in an incredibly high fracture toughness (Fleck and Qiu, 2007; Omidi and St-Pierre, 2023b).

With the objective of developing tougher lattice materials, we turn to nature for inspiration. Natural materials, such as wood and bone, are exceptionally tough, and this is usually attributed to the hierarchical design of biological materials (Launey and Ritchie, 2009). The concept of hierarchy is easily transferable to lattices, where it can be integrated in two ways. One approach is to introduce scaled-down patterns at the joints to produce fractal-like self-similar honeycombs, leading to improvements in stiffness, strength, and toughness (Ajdari et al., 2012; Haghpanah et al., 2013; Ryvkin and Shraga, 2018). Another avenue to introduce hierarchy in a lattice is to replace each cell wall by a smaller scale lattice. Prior studies have shown that this can increase the elastic modulus (Ma et al., 2016; Qing and Mishnaevsky, 2009; Taylor et al., 2011), buckling strength (Côte et al., 2009; Kazemahvazi et al., 2009;

* Corresponding author.
E-mail address: luc.st-pierre@aalto.fi (L. St-Pierre).

https://doi.org/10.1016/j.ijsolstr.2025.113374
Received 25 October 2024; Received in revised form 25 March 2025; Accepted 1 April 2025
Available online 9 April 2025

Table 1
Scaling constants for the fracture toughness of planar lattices (Fleck and Qiu, 2007).

Topology	D_I	D_{II}	d
Hexagonal	0.80	0.37	2
Triangular	0.50	0.38	1
Kagome	0.21	0.13	0.5

Table 2
Constants for the relative density of hierarchical lattices.

Large-scale topology	A	A_h	β_h
Hexagonal	$2/\sqrt{3}$	14/3	$4\sqrt{3}/21$
Triangular	$2\sqrt{3}$	14	$4\sqrt{3}/7$
Kagome	$\sqrt{3}$	7	$8\sqrt{3}/21$

Kooistra et al., 2005; Qing and Mishnaevsky, 2011; Vigliotti and Pasini, 2013; Wang et al., 2023; Yin et al., 2019), and energy absorption (Sun et al., 2016; Tran et al., 2014) of lattices. While these studies show that this form of hierarchy can be beneficial, a detailed analysis of its impact on fracture toughness is still missing.

This work aims to quantify the effect of hierarchy on the fracture toughness of planar lattices. Our scope is limited to three large-scale lattices: hexagonal, triangular, and Kagome lattices, as shown in Fig. 1a. These topologies are selected as they exhibit three different fracture behaviors as described above.

This article has the following structure: analytical modeling is presented in Section 2 and then compared to Finite Element (FE) simulations in Section 3. Then, further improvements are detailed in Section 4 using a functional grading approach and, finally, conclusions are listed in Section 5.

2. Analytical modeling

The hierarchical lattices considered in this work are shown in Fig. 1. They have two hierarchical levels, combining large- and small-scale lattices. We consider three large-scale architectures: hexagonal, Kagome, and triangular lattices. In all cases, the small-scale topology is a two-layer triangular lattice, see Fig. 1. This architecture was selected because it is structurally efficient (Torquato et al., 1998) and allows seamless joints for all three large-scale lattices. The geometry of each hierarchical lattice is therefore defined by three parameters: the beam length ℓ and thickness t, as well as the large-scale cell size L, see Fig. 1. The thickness of the hierarchical strut is related to the small-scale beam length via $c = \sqrt{3}\ell$.

The relative density of a hierarchical lattice is the product of the large- and small-scale relative densities. The large-scale relative density is given by:

$$\bar{\rho}_L = A\frac{c}{L}, \tag{2}$$

where A is a topology specific constant given in Table 2 for the three topologies examined in this study. Otherwise, the relative density of the small-scale triangular lattice is:

$$\bar{\rho}_\ell = \frac{7\sqrt{3}}{3}\left(\frac{t}{\ell}\right). \tag{3}$$

Note that the constant above is different from the value of A given in Table 2 for a triangular lattice. This discrepancy is to account for the fact that the small-scale lattice has only two cells in the transverse direction, whereas the value of A in Table 2 is representative of an infinite lattice. Finally, the overall relative density of a hierarchical lattice can be expressed as:

$$\bar{\rho} = \bar{\rho}_L\bar{\rho}_\ell f = A_h\frac{c}{L}\cdot\frac{t}{\ell}\left[1-\beta_h\frac{c}{L}\right], \tag{4}$$

where the constants A_h and β_h are given in Table 2, and the function f (in brackets above) accounts for the overlap of material at the joints. In general, it is adequate to assume $f \approx 1$, except for large values of c/L. For example, when $c/L = 0.2$ (the maximum value considered in this study), $f = 0.93$, 0.80, and 0.87 for hexagonal, triangular, and Kagome lattices, respectively.

Analytical predictions for the fracture toughness of hierarchical lattices are presented below for each topology and for both modes I and II. To derive these predictions, we start from the scaling law of simple lattices given in (1), and extend them to account for the mechanical properties of hierarchical struts. Therefore, this approach assumes that the behavior of the large-scale lattice is unaffected by the introduction of hierarchy. In line with the predictions in (1), we will consider that all lattices are made from an elastic-brittle material with a tensile strength σ_{ts}.

2.1. Hierarchical hexagonal lattice

A (non-hierarchical) hexagonal lattice is bending-dominated and therefore, its fracture toughness scales linearly with the maximum bending moment that the cell walls can support (Gibson and Ashby, 1997). Introducing hierarchy will increase the maximum bending moment and this enhancement will be proportional to the improvement in fracture toughness. Accordingly, the fracture toughness of a hierarchical hexagonal lattice can be expressed as:

$$K_{IC} = D_I\bar{\rho}_L^2\left(\frac{M_f^h}{M_f^s}\right)\sigma_{ts}\sqrt{L}, \tag{5}$$

where M_f^h and M_f^s are the bending moments at fracture for hierarchical and solid cell walls, respectively. The fracture moment of a hierarchical strut corresponds to the moment when the stress in the face sheets reaches the tensile strength of the solid σ_{ts}. Considering the hierarchical strut as a sandwich beam (see Fig. 1b), where $c \gg t$ and the core has negligible flexural rigidity, the fracture bending moment can be expressed as (Allen, 1969):

$$M_f^h = b_o c t \sigma_{ts}, \tag{6}$$

where b_o is the out-of-plane dimension of the lattice. Otherwise, the fracture moment of a solid strut of thickness c is given by Gibson and Ashby (1997):

$$M_f^s = \frac{I_s\sigma_{ts}}{y} = \frac{1}{6}b_o c^2\sigma_{ts}. \tag{7}$$

Using the small-scale relative density $\bar{\rho}_\ell$ defined in (3), the ratio M_f^h/M_f^s becomes:

$$\frac{M_f^h}{M_f^s} = \frac{6t}{c} = \frac{6t}{\sqrt{3}\ell} = \frac{6}{7}\bar{\rho}_\ell. \tag{8}$$

Substituting this in (5), using expression (2), and assuming $\bar{\rho} \approx \bar{\rho}_L\bar{\rho}_\ell$, returns the mode I fracture toughness of a hierarchical hexagonal lattice:

$$\frac{K_{IC}}{\sigma_{ts}\sqrt{L}} = 0.79\left(\frac{c}{L}\right)\bar{\rho}. \tag{9}$$

Otherwise, the mode II fracture toughness is obtained simply by replacing D_I by D_{II} in (5) and this gives:

$$\frac{K_{IIC}}{\sigma_{ts}\sqrt{L}} = 0.37\left(\frac{c}{L}\right)\bar{\rho}. \tag{10}$$

The above equations show that introducing hierarchy can significantly increase the fracture toughness of a hexagonal lattice. First, hierarchy modifies the scaling with relative density from $\bar{\rho}^2$ to $\bar{\rho}$. Second, the fracture toughness of a hierarchical design increases linearly with the stockiness c/L of the large-scale lattice, which allows to increase the fracture toughness while keeping the relative density fixed.

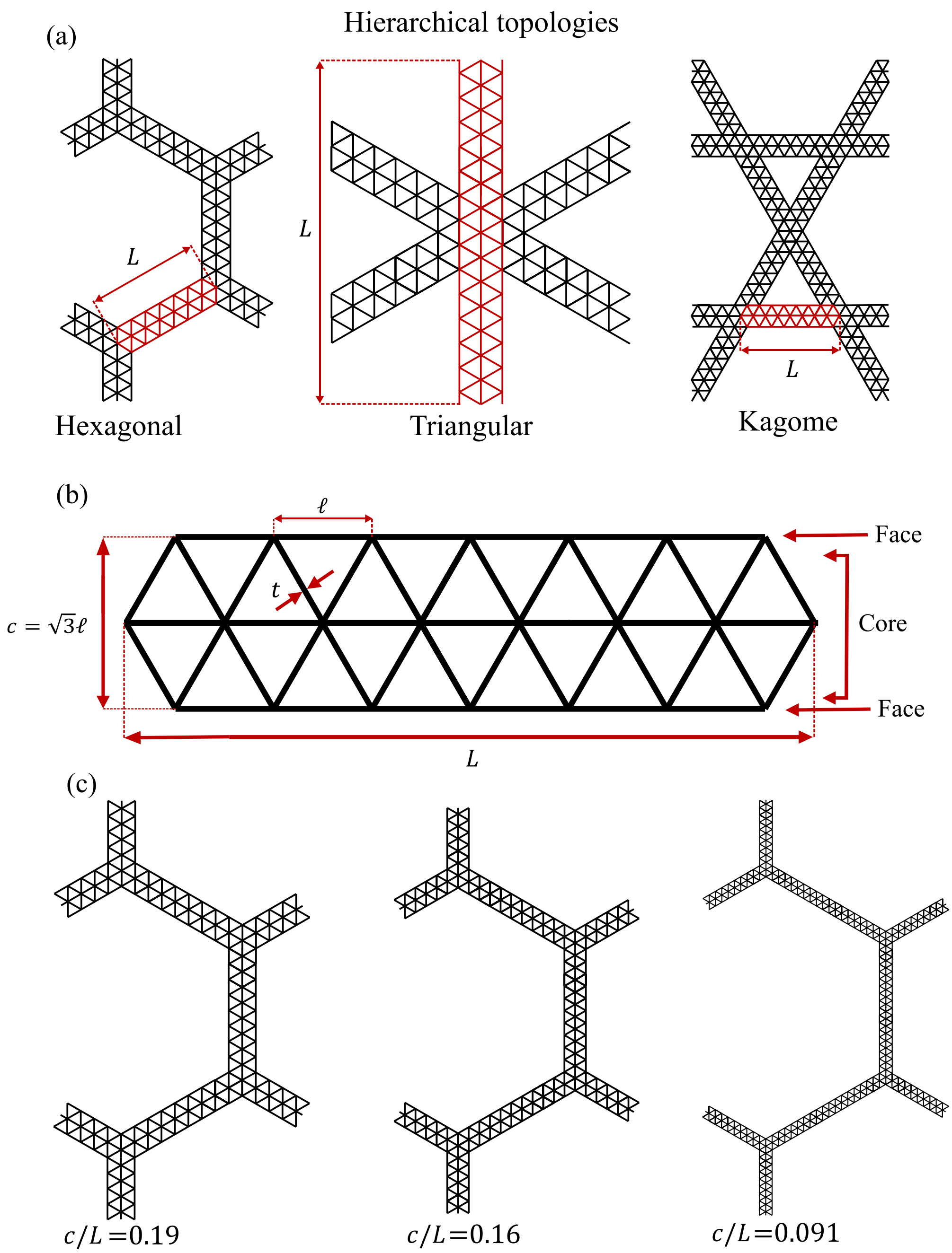

Fig. 1. (a) Unit cells of hierarchical topologies. (b) Geometry of a single hierarchical strut. (c) Evolution of a hierarchical hexagonal lattice for three values of stockiness c/L.

2.2. Hierarchical triangular lattice

A simple triangular lattice is stretching-dominated, and its fracture toughness is dictated by the tensile strength σ_{ts} of the cell walls (Fleck and Qiu, 2007). Therefore, we can estimate the fracture toughness of a hierarchical triangular lattice by replacing σ_{ts} in (1) by the tensile strength of a hierarchical strut. This gives:

$$K_{IC} = D_I \bar{\rho}_L \sigma_{ts}^h \sqrt{L}, \tag{11}$$

where σ_{ts}^h is the longitudinal tensile strength of a hierarchical strut. Assuming that the load is carried by the three longitudinal bars (see Fig. 1b), σ_{ts}^h can be expressed as:

$$\sigma_{ts}^h = \frac{3t}{c}\sigma_{ts} = 0.43\bar{\rho}_\ell \sigma_{ts}. \tag{12}$$

Note that this result is slightly higher than the strength of a triangular lattice because of size effects (Gu et al., 2018). We then substitute (12) in (11), and use the approximation $\bar{\rho} \approx \bar{\rho}_L \bar{\rho}_\ell$, to obtain the mode I fracture toughness of a hierarchical triangular lattice:

$$\frac{K_{IC}}{\sigma_{ts}\sqrt{L}} = 0.215\bar{\rho}. \tag{13}$$

Repeating the same procedure for mode II (replace D_I by D_{II} in (11)) returns:

$$\frac{K_{IIC}}{\sigma_{ts}\sqrt{L}} = 0.163\bar{\rho}. \tag{14}$$

Comparing these predictions to (1) shows that hierarchy decreases the fracture toughness of a triangular lattice by 57% for both modes. This is not surprising since the tensile strength of a hierarchical strut is lower than that of a fully-dense cell wall, see (12). Nonetheless, both simple

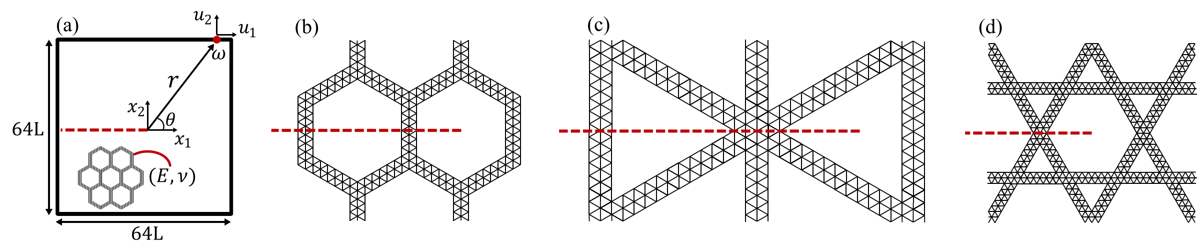

Fig. 2. (a) Domain used in FE simulations. Location of the initial crack (dashed red line) for hierarchical (b) hexagonal, (c) triangular, and (d) Kagome lattices.

and hierarchical triangular lattices have a fracture toughness that scales linearly with relative density.

2.3. Hierarchical Kagome lattice

The Kagome lattice is also stretching-dominated; therefore, the fracture toughness of its hierarchical design can be estimated following the approach used in Section 2.2 for a triangular lattice. Replacing the tensile strength of a cell wall σ_{ts} in (1) by the tensile strength of a hierarchical strut σ_{ts}^h gives:

$$K_{IC} = D_I \sqrt{\bar{\rho}_L} \sigma_{ts}^h \sqrt{L}. \tag{15}$$

Next, we substitute σ_{ts}^h from (12), use the definition of $\bar{\rho}_L$ given in (2), and the approximation $\bar{\rho} \approx \bar{\rho}_L \bar{\rho}_\ell$ to get the mode I fracture toughness of a hierarchical Kagome lattice:

$$\frac{K_{IC}}{\sigma_{ts}\sqrt{L}} = \frac{0.069}{\sqrt{c/L}} \bar{\rho}. \tag{16}$$

Repeating the same procedure for mode II returns:

$$\frac{K_{IIC}}{\sigma_{ts}\sqrt{L}} = \frac{0.043}{\sqrt{c/L}} \bar{\rho}. \tag{17}$$

Comparing these expressions with (1) indicates that introducing hierarchy changes the scaling from $\sqrt{\bar{\rho}}$ to $\bar{\rho}$. In addition, the fracture toughness of a hierarchical Kagome lattice is predicted to increase when c/L decreases. It should be noted that the Kagome lattice brings a unique challenge when deriving analytical predictions because, even though its behavior is stretching-dominated, it exhibits a crack tip blunting phenomenon, which causes local bending deformations (Fleck and Qiu, 2007). The importance of this phenomenon in a hierarchical Kagome lattice will be discussed later in Section 3.4.

3. Finite element predictions

3.1. Description of the modeling approach

Finite Element (FE) simulations were conducted to verify the analytical expressions presented in Section 2. All simulations were preformed using the finite element package Abaqus; we used the implicit solver and assumed small strain theory. The fracture toughness was predicted using the boundary layer method, which was first introduced by Schmidt and Fleck (2001) and used extensively in subsequent studies (Fleck and Qiu, 2007; Omidi and St-Pierre, 2023a,b; Romijn and Fleck, 2007; Tankasala et al., 2015; Yang and Zhang, 2024). Using this approach ensures that our results are directly comparable to those of non-hierarchical topologies given in Table 1.

A square domain, with a side length of roughly $64L$, was created for each hierarchical lattice, see Fig. 2a. This domain contained an initial crack positioned along the negative x_1-axis, with the precise location of the crack tip and orientation of the lattice given in Fig. 2b–d. Preliminary simulations, reported in Appendix A.1, showed that this domain is sufficiently large to ensure that the fracture toughness predictions are independent of the domain size. The influence of the lattice orientation was also investigated for all topologies, and we found that this had a negligible effect on the fracture toughness, see Appendix A.2. The straight initial cracks considered here are representative of those used in fracture toughness tests. In reality, cracks nucleating and propagating are likely to follow a tortuous path in these hierarchical lattices. While it is impossible to study all possibilities, we show, in Appendix A.3, that changing the straight initial cracks to more realistic patterns has a negligible effect on our predictions.

All hierarchical lattices were meshed with Timoshenko beam elements (B21 in Abaqus). Ten elements per strut ℓ were used around the crack tip ($r < 3L$, see Fig. 2a), and the number of elements per strut was gradually decreased to three on the outer boundary of the domain. A mesh convergence study showed that further mesh refinements had a negligible effect on the results, see Appendix A.1. Simulations were performed for relative densities ranging from 0.005 to 0.1 and for large-scale stockiness c/L varying from 0.06 to 0.20, see Fig. 1c. This was done by changing the small-scale bar thickness t and the large-scale cell size L, while keeping the small-scale strut length ℓ fixed. In all cases, the relative density was calculated with (4).

The three hierarchical lattices have a six-fold rotational symmetry; therefore, their elastic proprieties are transversely isotropic. Consequently, each node on the boundary of the domain was prescribed a displacement (u_1, u_2) and rotation ω in accordance with the crack tip field in an isotropic elastic solid (Fleck and Qiu, 2007):

$$u_1 = \frac{K_I}{2\sqrt{2\pi}G}\sqrt{r}(\kappa - \cos\theta)\cos\frac{\theta}{2} + \frac{K_{II}}{2\sqrt{2\pi}G}\sqrt{r}(\kappa + 2 + \cos\theta)\sin\frac{\theta}{2}, \tag{18a}$$

$$u_2 = \frac{K_I}{2\sqrt{2\pi}G}\sqrt{r}(\kappa - \cos\theta)\sin\frac{\theta}{2} - \frac{K_{II}}{2\sqrt{2\pi}G}\sqrt{r}(\kappa - 2 + \cos\theta)\cos\frac{\theta}{2}, \tag{18b}$$

$$\omega = \frac{1+\kappa}{4\sqrt{2\pi}G}\sqrt{r}(K_I \sin\frac{\theta}{2} + K_{II}\cos\frac{\theta}{2}), \tag{18c}$$

where (r, θ) are polar coordinates originating from the crack tip; $\kappa = (3 - \nu_{ps})/(1 + \nu_{ps})$; G is the effective shear modulus and ν_{ps} is the plane strain Poisson's ratio of the lattice, which is given in Appendix B for each topology. Otherwise, K_I and K_{II} are the stress intensity factors for modes I and II, respectively.

In all cases, the lattices were considered to be made from an elastic-brittle material, characterized by an elastic modulus E_s and a Poisson's ratio ν_s. The simulations were performed under plane strain and this required to modify the material properties of each beam element as follows (Fleck and Qiu, 2007):

$$E_s' = \frac{E_s}{1 - \nu_s^2} \quad \text{and} \quad \nu_s' = \frac{\nu_s}{1 - \nu_s}. \tag{19}$$

We adopted the point-wise failure criterion, which assumes that the fracture toughness K_{IC} (or K_{IIC}) corresponds to the value of K_I (or K_{II}) when the maximum local tensile stress reaches the strength σ_{ts} of the solid (Tankasala et al., 2015). The point-wise failure criterion is suitable for lattices made from an elastic-brittle material, which fractures immediately after the tensile stress reaches a critical value (Mangipudi and Onck, 2011; Onck et al., 2004).

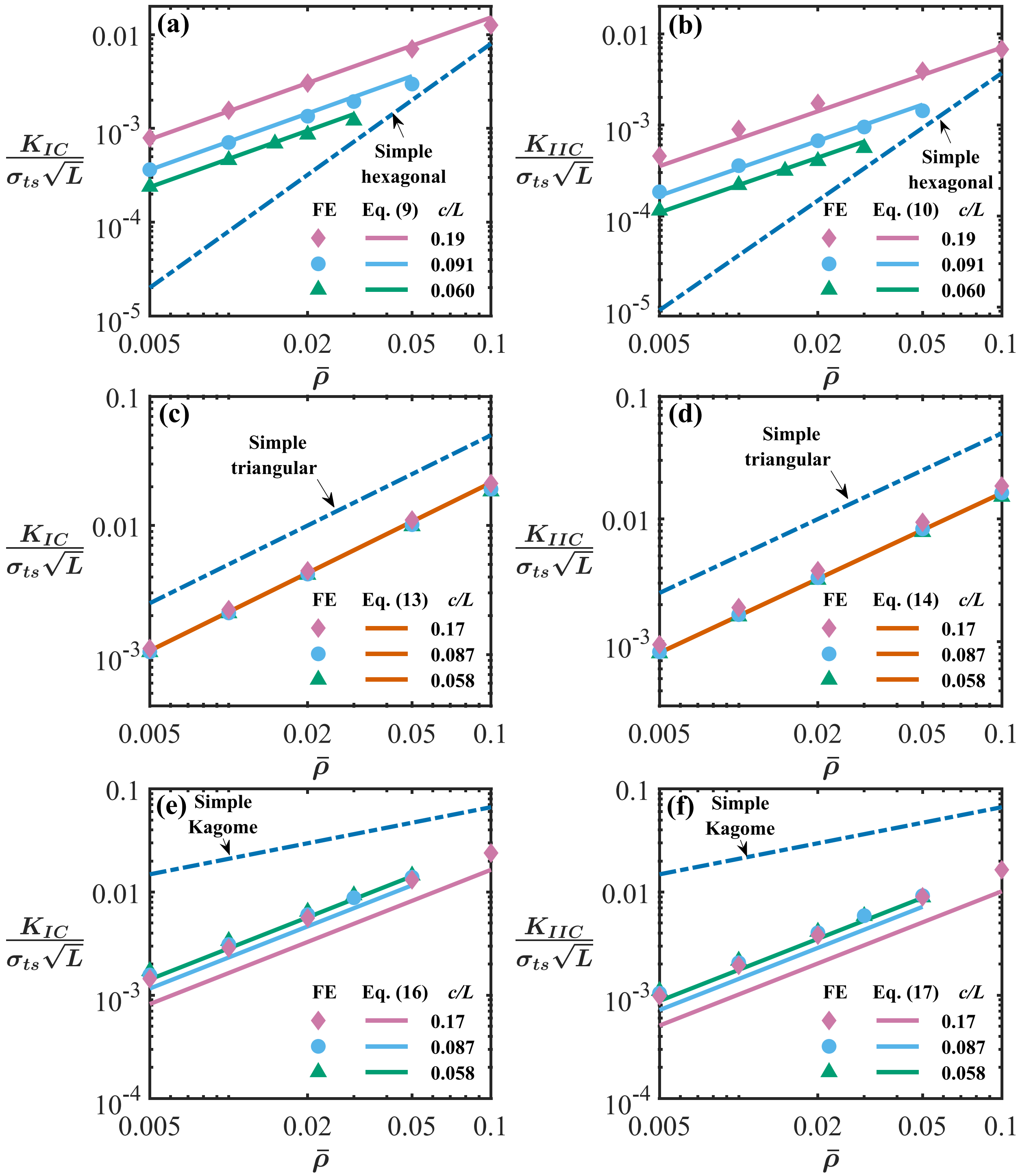

Fig. 3. Normalized fracture toughness as a function of relative density for a hierarchical hexagonal lattice under (a) mode I and (b) mode II. Likewise, results are given for a hierarchical triangular lattice under (c) mode I and (d) mode II; and a hierarchical Kagome lattice under (e) mode I and (f) mode II. In each plot, the toughness of a simple, non-hierarchical lattice is included for comparison.

3.2. Comparison between finite element and analytical predictions

The normalized fracture toughness is plotted in Fig. 3 as a function of relative density for the three hierarchical designs considered in this work and for both modes I and II. In each plot, FE simulations are compared to analytical predictions for three selected values of c/L. Since both our analytical and numerical modeling rely on beam theory, we limited our attention to slender geometries where $t/\ell < 0.125$. This restriction explains why data for low values of c/L does not span the entire range of relative densities (see, for example, the results for $c/L = 0.060$ in Fig. 3a). Each plot also includes, for comparison, the fracture toughness of a non-hierarchical topology given by (1). Finally, we emphasize that the fracture toughness of both non-hierarchical and hierarchical lattices is normalized by the large-scale cell size L to ensure a fair comparison between both designs.

The fracture toughness of a hierarchical hexagonal lattice is shown in Fig. 3a and b for mode I and II, respectively. Clearly, hierarchical designs are significantly tougher than a conventional hexagonal lattice.

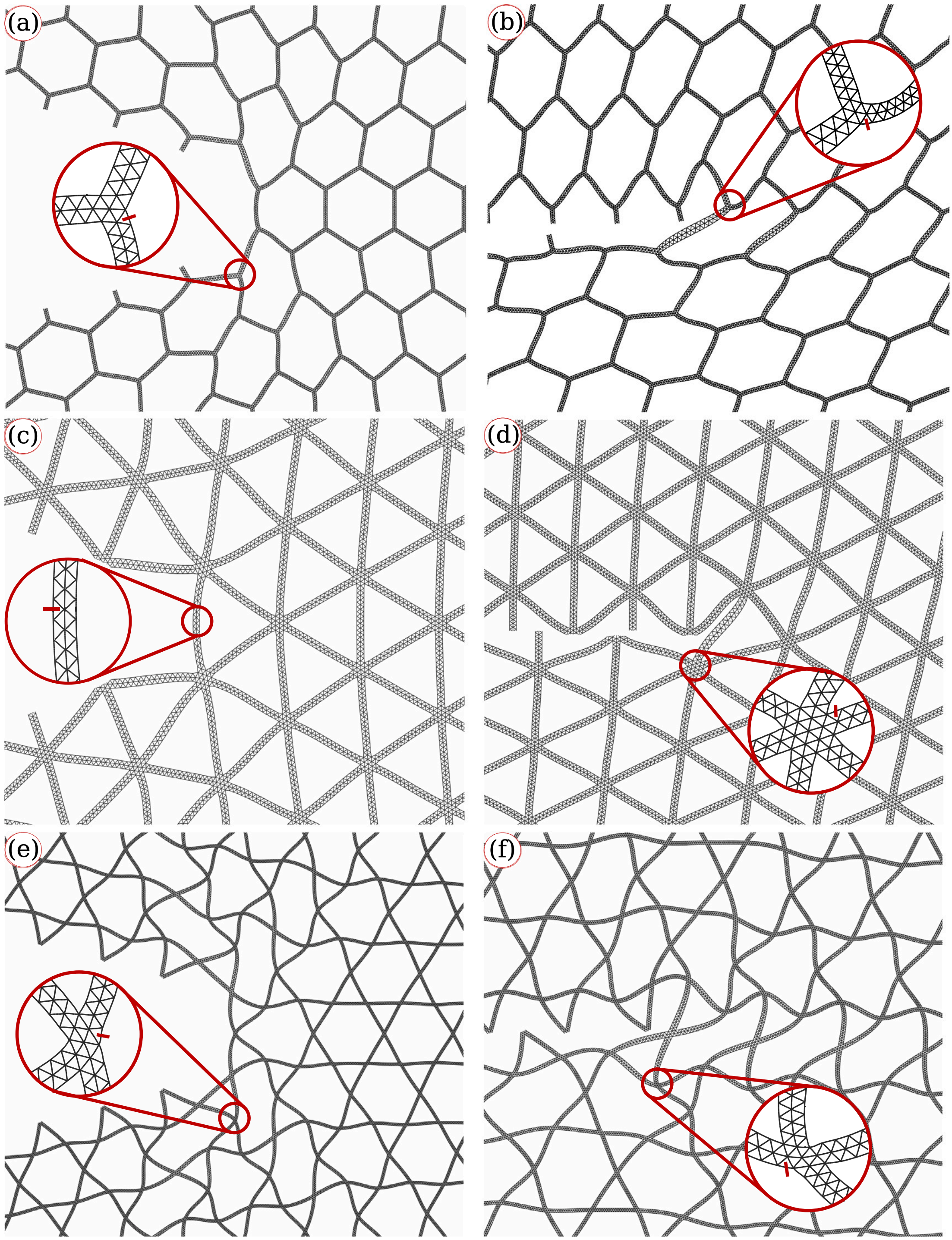

Fig. 4. Location of the first cell wall to fracture in a hierarchical hexagonal lattice under (a) mode I and (b) mode II. Likewise, results are given for a hierarchical triangular lattice under (c) mode I and (d) mode II; and a hierarchical Kagome lattice under (e) mode I and (f) mode II. All lattices have $\bar{\rho} = 0.05$ and $c/L \approx 0.09$, and the deformed meshes have exaggerated displacements to emphasize the deformation mode.

This increase in toughness is more important at low relative densities since the toughness of a hierarchical design scales linearly with relative density whereas that of a simple hexagonal lattice scales as $\bar{\rho}^2$, see Table 1. The fracture toughness of a hierarchical hexagonal lattice also increases linearly with the large-scale stockiness c/L. This is consistent with the fact that increasing c/L increases the bending strength of hierarchical cell walls. For both modes I and II, there is a very good agreement between analytical and FE predictions.

Results for a hierarchical triangular lattice are shown in Fig. 3c for mode I and in Fig. 3d for mode II. Here, introducing hierarchy decreases the fracture toughness by about 50% for both modes I and II. Despite this reduction, both simple and hierarchical triangular lattices maintain a toughness that scales linearly with relative density. Again, there is an excellent agreement between FE simulations and analytical predictions, and this holds true for both modes I and II.

The fracture toughness of a hierarchical Kagome lattice is given in Fig. 3e and f for mode I and mode II, respectively. Introducing hierarchy significantly lowers the toughness of a Kagome lattice, and this is more important at low relative densities. This is due to the fact that the toughness of a simple Kagome lattice scales as $\sqrt{\bar{\rho}}$ whereas that of its

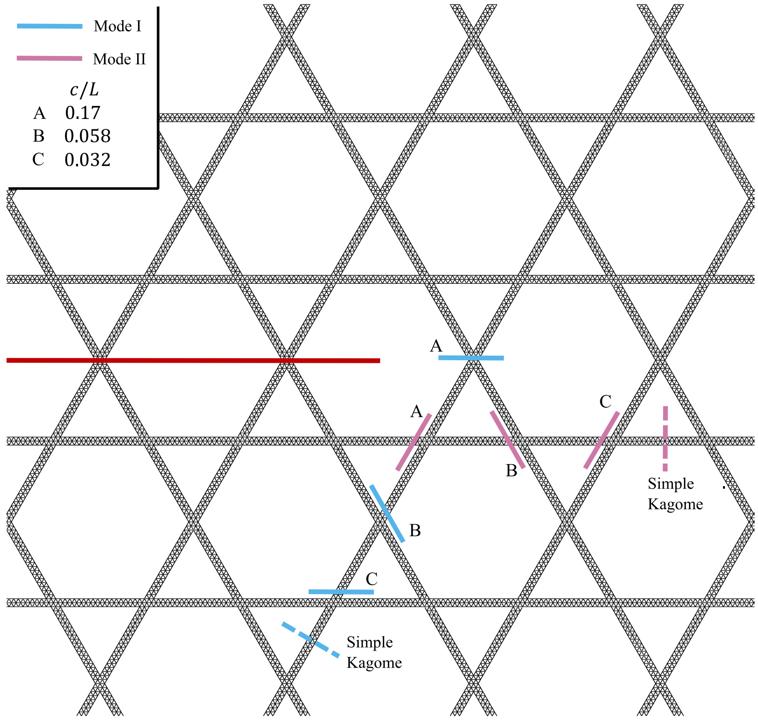

Fig. 5. Evolution of the failure location in a hierarchical Kagome lattice for three selected values of large-scale stockiness c/L. Results are given for both modes I and II. The fracture site in a simple, non-hierarchical Kagome lattice (taken from Fleck and Qiu (2007)) is also included for comparison.

hierarchical counterpart scales as $\bar{\rho}$. While this change in the scaling law is predicted by our analytical model (see Section 2.3), it is clear from Fig. 3e,f that the effect of c/L is not captured accurately in our analytical predictions. Our analytical model predicts a 70% increase in fracture toughness when the stockiness c/L is changed from 0.17 to 0.058, but our FE simulations show a modest increase of 20% only. The mechanisms leading to this discrepancy are investigated below, in Section 3.4.

3.3. Deformed meshes and fracture locations

The location of the first cell wall to fracture is given in Fig. 4 for each hierarchical lattice and for both modes I and II. Results are shown for $c/L \approx 0.09$ and $\bar{\rho} = 0.05$, but the failure location is insensitive to $\bar{\rho}$. Both hierarchical hexagonal and triangular lattices have a fracture location that is close to the crack tip under both modes I and II, see Fig. 4a–d. For these two topologies, the fracture site is independent of c/L and corresponds to the same failure location as in their simple, non-hierarchical counterparts, see Fleck and Qiu (2007). This indicates that the large-scale behavior of hexagonal and triangular lattices is unaffected by the introduction of hierarchy. In contrast, the failure location in a hierarchical Kagome lattice is sensitive to the large-scale stockiness c/L. This is shown in Fig. 5, where the fracture site is given for three selected values of c/L. The failure location in a simple, non-hierarchical Kagome lattice (taken from Fleck and Qiu (2007)) is also included for comparison. For both modes I and II, the fracture site in a hierarchical Kagome lattice moves away from the crack tip (and closer to the failure site in a simple Kagome lattice) when c/L decreases.

3.4. Discussion on the toughness of a hierarchical Kagome lattice

The comparison between analytical and FE results in Fig. 3 showed that, while there is a good agreement for hierarchical hexagonal and triangular lattices, an important discrepancy exists for the Kagome topology. This section aims to find the cause of this deviation and revise our analytical predictions for the fracture toughness of hierarchical Kagome lattices.

A simple, non-hierarchical Kagome lattice has a very peculiar fracture behavior: its deformation is stretching-dominated far from the crack tip, whereas there is a combination of bar bending and stretching closer to the crack tip, and this area is referred to as the blunting zone (Fleck and Qiu, 2007). Therefore, we first investigate if a crack tip blunting zone exists in hierarchical Kagome lattices by inspecting the deformed meshes for two values of stockiness c/L, see Fig. 6. Clearly, c/L has a huge effect on the blunting zone: the stocky construction with $c/L = 0.17$ shows almost no blunting (see Fig. 6a), whereas the slender design with $c/L = 0.058$ has a pronounced blunting zone emanating from the crack tip (see Fig. 6b).

We can quantify the extent of the blunting zone with the metric proposed by Fleck and Qiu (2007). They measured the blunting zone as the radial distance r_{el} from the crack tip over which the absolute node rotation $|\omega|$ exceeds $K_I/(E\sqrt{L})$ (where E is the elastic modulus of the lattice given in Appendix B; for mode II, simply replace K_I by K_{II}). The normalized blunting zone r_{el}/L is plotted in Fig. 7 as a function of $\bar{\rho}_L$ for hierarchical Kagome lattices. The data for both modes I and II collapses on a single trendline given by:

$$\frac{r_{el}}{L} = \frac{1}{4\,\bar{\rho}_L^{1.5}}. \tag{20}$$

The normalized blunting zone for a simple, non-hierarchical Kagome lattice is also included in Fig. 7 for comparison. These results are reproduced from Fleck and Qiu (2007), and $\bar{\rho} = \bar{\rho}_L$ for a simple, non-hierarchical lattice. Clearly, introducing hierarchy slightly reduces the size of the blunting zone, but $r_{el} \propto L/\bar{\rho}_L^{1.5}$ for both simple and hierarchical designs.

Next, we shall make use of the blunting zone in (20) to revise our analytical prediction for the fracture toughness of a hierarchical Kagome lattice. Our approach is similar to that used by Fleck and Qiu (2007) for a simple, non-hierarchical Kagome lattice: we assume that the fracture toughness is governed by the bending strength of a cell wall located at a distance r_{el} from the crack tip. Consider a hierarchical

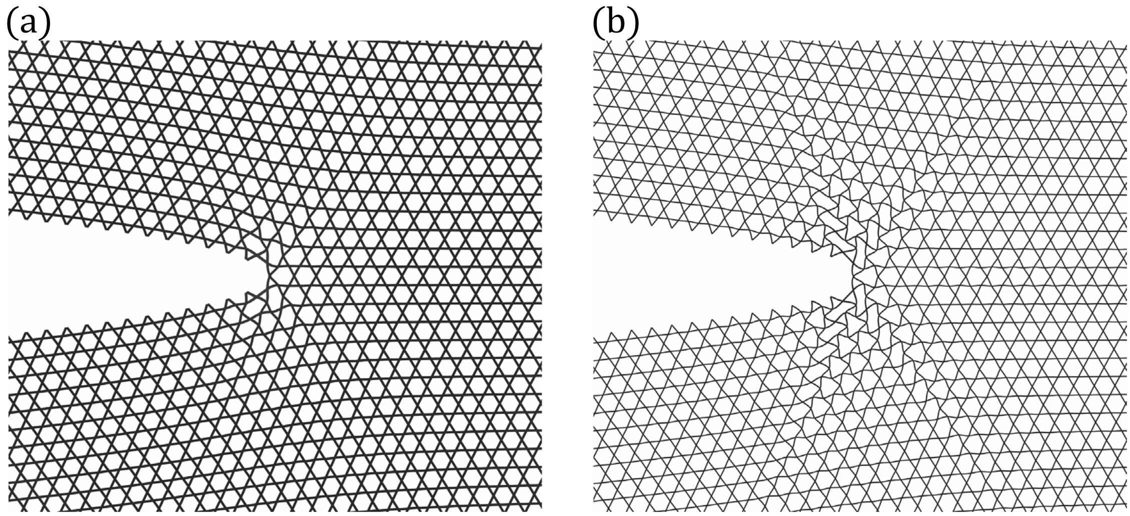

Fig. 6. Deformed meshes for hierarchical Kagome lattices with $\bar{\rho} = 0.05$ and a large-scale stockiness ratio (a) $c/L = 0.17$ and (b) $c/L = 0.058$. This shows that the blunting zone decreases with increasing c/L.

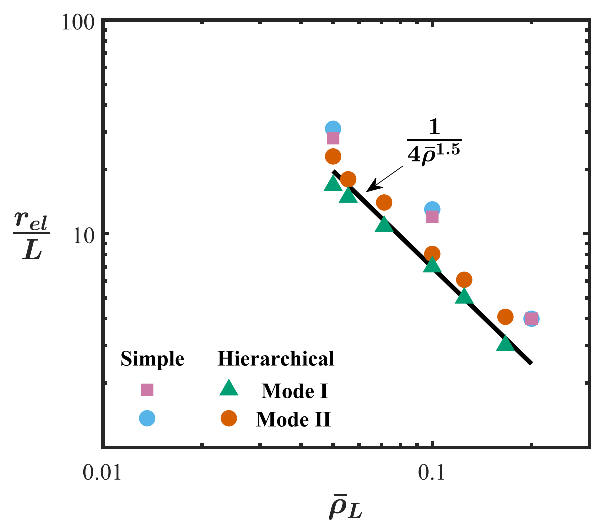

Fig. 7. Hierarchical and simple Kagome normalized crack tip deformation zone with $\bar{\rho} = 0.02$, where simple Kagome data is from Fleck and Qiu (2007).

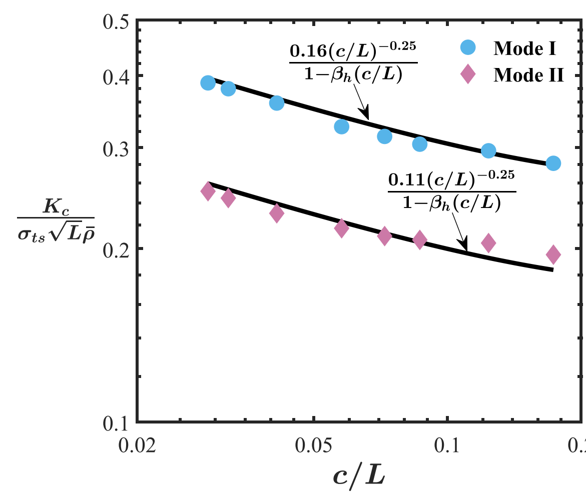

Fig. 8. Normalized fracture toughness as a function of c/L for hierarchical Kagome lattices. Results are shown for both modes I and II.

strut that is fixed on one end and subjected to a displacement δ at the other end. The maximum bending stress at the root of the cantilever is then given as $\sigma_b \approx \delta E_s c/L^2$. Setting $\sigma_b = \sigma_{ts}$ and the displacement $\delta = K_{IC}\sqrt{r_{el}}/E$, where $E \approx \bar{\rho}_L \bar{\rho}_\ell E_s$, gives a revised prediction for the mode I fracture toughness of a hierarchical Kagome lattice:

$$\frac{K_{IC}}{\sigma_{ts}\sqrt{L}} = C_1 \left(\frac{c}{L}\right)^{-0.25} \cdot \bar{\rho} \cdot f^{-1} = \frac{C_1 (c/L)^{-0.25}}{1-\beta_h(c/L)}\,\bar{\rho}, \tag{21}$$

where C_1 is a constant of proportionality, whereas f and $\beta_h = 8\sqrt{3}/21$ were introduced earlier in (4). To verify this prediction, $K_{IC}/(\bar{\rho}\sigma_{ts}\sqrt{L})$ is plotted as a function of c/L in Fig. 8. The FE simulations are in good agreement with (21) when the constant of proportionality $C_1 = 0.16$. Repeating the analysis for mode II gives the same scaling as in (21), but with a slightly lower constant of proportionality, see Fig. 8. Note that for $c/L < 0.08$, it is reasonable to assume $f \approx 1$ in (21), which returns a simpler scaling law: $K_{IC} \propto (c/L)^{-0.25}\,\bar{\rho}\,\sigma_{ts}\sqrt{L}$. However, this assumption is not valid for higher values of c/L and this introduces an additional term in the prediction.

In summary, both simple and hierarchical Kagome lattices exhibit a similar behavior: they both have a blunting zone r_{el} that decreases with increasing $\bar{\rho}_L$. Hierarchy, however, slightly reduces r_{el} (see Fig. 7) and leads to a different scaling than that previously obtained by Fleck and Qiu (2007). Those differences explain the discrepancy between analytical and FE predictions introduced earlier in Fig. 3e,f.

4. Functional grading of hierarchical hexagonal lattice

The results in Fig. 3 demonstrate that hierarchy can significantly increase the fracture toughness of a hexagonal lattice. This enhancement is due to the fact that hierarchical struts have a higher bending strength than fully-dense cell walls, when compared on an equal mass basis. The benefits of hierarchy can be increased further by re-distributing mass from the core to the faces of the hierarchical strut, which is quantified below.

Consider the functionally graded, hierarchical hexagonal lattice shown in Fig. 9, where the faces have a thickness t_f and the bars in the core, a thickness t_c. In this design, the joints are made from bars with a thickness t_f to prevent localized deformation. The small-scale relative density of this functionally graded design is given by:

$$\bar{\rho}_\ell = \frac{2t_f + 5t_c}{\sqrt{3}\ell} = \frac{(2\bar{t}+5)}{\sqrt{3}\bar{t}}\,\frac{t_f}{\ell}, \tag{22}$$

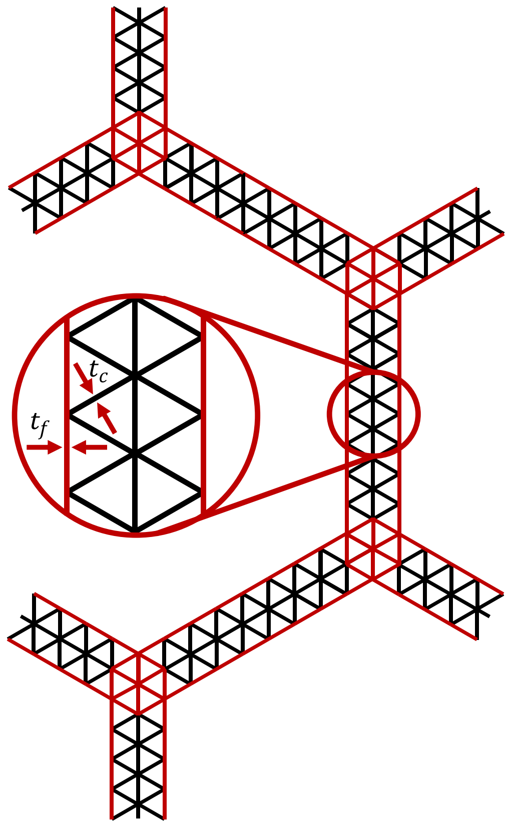

Fig. 9. A functionally graded hierarchical hexagonal lattice where the bars in red have a thickness t_f and those in black, a thickness t_c.

where the ratio $\bar{t} = t_f/t_c$. Otherwise, the large-scale relative density remains unchanged, see (2), and the overall relative density becomes:

$$\bar{\rho} = \bar{\rho}_L \bar{\rho}_\ell f = \frac{2}{3} \frac{(2\bar{t}+5)}{\bar{t}} \frac{c}{L} \frac{t_f}{\ell} \left[1 - \frac{2}{\sqrt{3}} \frac{(5-3\bar{t})}{(5+2\bar{t})} \frac{c}{L} \right]. \tag{23}$$

In this case, the bending moment causing fracture of a hierarchical strut is given by:

$$M_f^h = b_o c t_f \sigma_{ts}, \tag{24}$$

and the enhancement ratio M_f^h/M_f^s (where M_f^s is defined in (7)) becomes:

$$\frac{M_f^h}{M_f^s} = \frac{6t_f}{c} = \frac{6\bar{t}}{2\bar{t}+5} \bar{\rho}_\ell. \tag{25}$$

Substituting this in (5), and assuming $\bar{\rho} \approx \bar{\rho}_L \bar{\rho}_\ell$, gives the mode I fracture toughness of a graded hierarchical hexagonal lattice:

$$\frac{K_{IC}}{\sigma_{ts}\sqrt{L}} = \frac{5.54\,\bar{t}}{(2\bar{t}+5)} \left(\frac{c}{L}\right) \bar{\rho}. \tag{26}$$

Similarly, the mode II fracture toughness is obtained by replacing D_I by D_{II} in (5) and this gives:

$$\frac{K_{IIC}}{\sigma_{ts}\sqrt{L}} = \frac{2.56\,\bar{t}}{(2\bar{t}+5)} \left(\frac{c}{L}\right) \bar{\rho}. \tag{27}$$

Additional FE simulations were conducted to corroborate these analytical predictions. These simulations were done using the same modeling approach outlined in Section 3.1, but the elastic properties of the graded lattice (G and ν_{ps}) were obtained from separate FE simulations using a periodic unit cell. Analytical and FE predictions are compared in Fig. 10 for $\bar{t}$ = 1, 2, and 4. The fracture toughness of a panel with $c/L = 0.091$ is given in Fig. 10a and b for modes I and II, respectively. Likewise, results for $c/L = 0.060$ are given in Fig. 10c for mode I and in Fig. 10d for mode II. In each plot, FE results are reported for two different fracture criteria: LTS and ATS. Since beam elements are used, they have a linear distribution of stresses through the thickness, characterized by an average σ_A and a maximum tensile value σ_T on the outermost fiber. The maximum local stress (LTS) criterion assumes that fracture occurs when $\sigma_T = \sigma_{ts}$ (this is the approach used previously in this paper). In contrast, the average tensile stress (ATS) criterion considers that failure occurs when $\sigma_A = \sigma_{ts}$. A similar approach was used previously by Tankasala et al. (2015), and it is useful here to distinguish if the critical element is loaded primarily in tension or with a combination of tensile and bending stresses.

The results in Fig. 10 show that fracture toughness roughly doubles as $\bar{t}$ is increased from 1 to 4. In general, there is a good agreement between analytical predictions and FE simulations, especially those relying on the ATS criterion. At low relative densities, the LTS and ATS criteria yield similar predictions, indicating that the critical element is loaded primarily in tension, with negligible bending stresses. Bending stresses, however, increase with increasing $\bar{\rho}$ and $\bar{t}$, leading to significant differences between the LTS and ATS criteria at high relative densities and $\bar{t} = 4$. Note that the failure location is not sensitive to $\bar{t}$ or the choice of fracture criterion. Even though the LTS predictions are below those obtained with the ATS criterion, the results demonstrate that increasing $\bar{t}$ can significantly increase fracture toughness under both modes I and II.

5. Conclusion

The mode I and mode II fracture toughness of hierarchical hexagonal, triangular, and Kagome lattices was investigated using FE simulations and analytical modeling. Our findings indicate that hierarchy provides significant benefits to the fracture toughness of the hexagonal lattice, which is bending-dominated. This is attributed to the increase in bending strength of the cell walls. In addition, hierarchy causes an important change in scaling: the fracture toughness of a hierarchical hexagonal lattice scales linearly with relative density, whereas $K_{IC} \propto \bar{\rho}^2$ for its non-hierarchical counterpart. This change in scaling leads to a substantially higher fracture toughness, particularly at low relative densities. The fracture toughness of a hierarchical hexagonal lattice can be improved further by functional grading: moving mass from the core to the faces of the hierarchical cell walls. This approach can double the fracture toughness if the faces are four times thicker than the core members.

In contrast, hierarchy did not improve the fracture toughness of stretching-dominated topologies such as triangular and Kagome lattices. Hierarchy has a fairly small effect on the performances of a triangular lattice, as both simple and hierarchical designs have a fracture toughness that scales linearly with relative density. Hierarchy, however, has a more pronounced effect on the Kagome lattice: it slightly reduces the crack tip blunting phenomenon and affects the fracture location. This leads to a change in scaling: the fracture toughness $K_{IC} \propto \bar{\rho}$ for a hierarchical Kagome lattice, whereas it scales with $\sqrt{\bar{\rho}}$ for its simple, non-hierarchical counterpart.

Natural lightweight materials, like wood and bone, have a high toughness, which is usually attributed to their hierarchical construction. These natural materials are bending-dominated and therefore, hierarchy is an excellent strategy to increase their fracture toughness, as demonstrated in this study. Future work should explore other potential benefits of hierarchical lattices. For example, at low relative densities, elastic buckling may occur before tensile fracture in stretching-dominated lattices (Shaikeea et al., 2022). Hierarchy can delay this transition and increase the performances of lattices at low relative densities. Hierarchy could also provide additional resistance to crack propagation by activating crack bridging and microcracking, which are not present in simple, non-hierarchical lattices (Hsieh et al., 2020; Tankasala and Fleck, 2020; Hedvard et al., 2024).

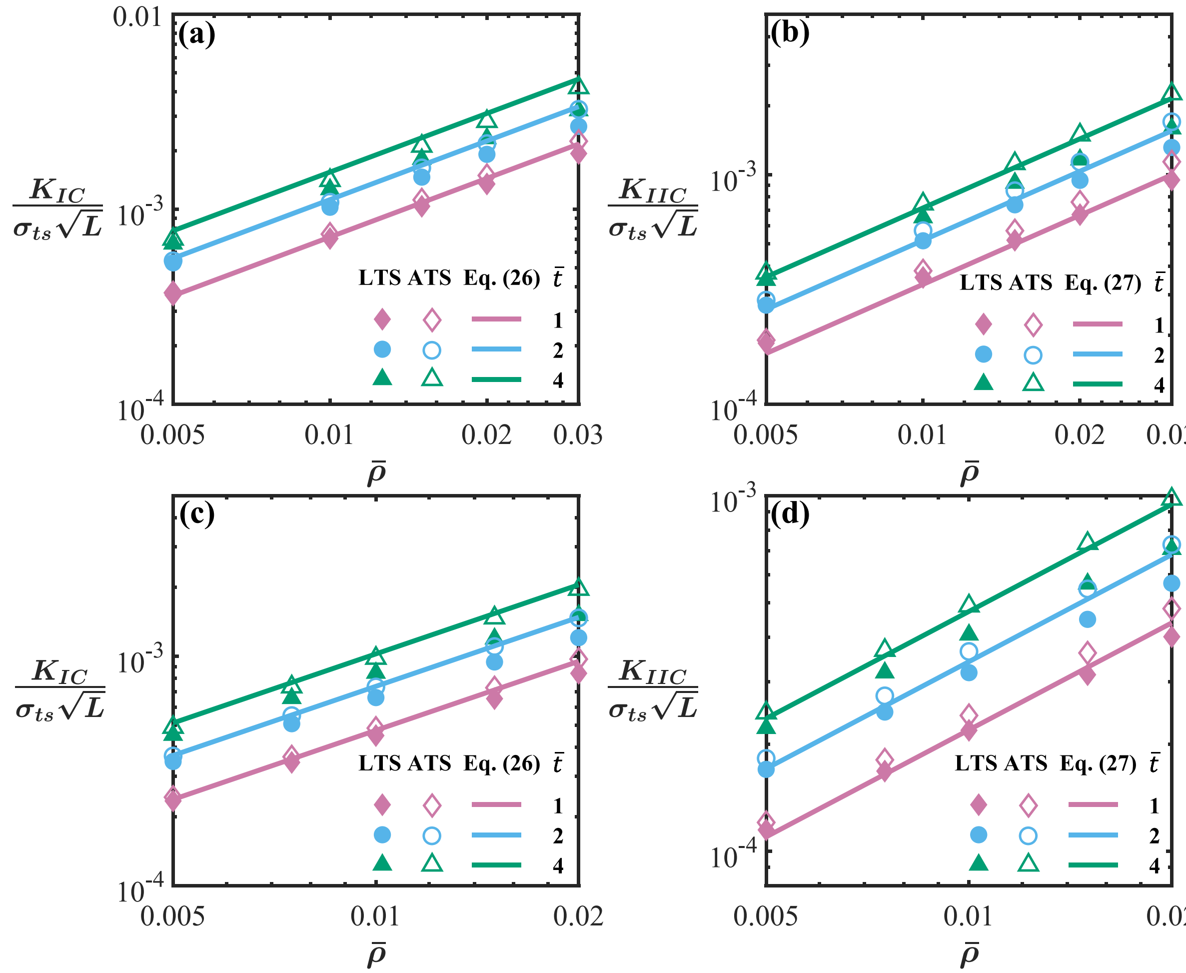

Fig. 10. Normalized fracture toughness as a function of relative density for a functionally graded, hierarchical hexagonal lattice with $c/L = 0.091$ under (a) mode I and (b) mode II. Likewise, results are given for $c/L = 0.060$ under (c) mode I and (d) mode II. FE results are reported for two different fracture criteria: the maximum local stress (LTS) and the average tensile stress (ATS).

CRediT authorship contribution statement

Akseli Leraillez: Writing – original draft, Visualization, Validation, Methodology, Investigation, Funding acquisition, Formal analysis, Conceptualization. **Luc St-Pierre:** Writing – review & editing, Supervision, Methodology, Funding acquisition, Conceptualization.

Declaration of competing interest

The authors declare that they have no known competing financial interests or personal relationships that could have appeared to influence the work reported in this paper.

Acknowledgments

This work was supported by the Academy of Finland (decision 322007). AL is grateful for the financial support of the Finnish Cultural Foundation (decision 0024078).

Appendix A. Modeling considerations

A.1. Influence of domain and mesh sizes

Finite Element predictions were conducted to verify that the domain and mesh sizes were adequate. These simulations were done for a hierarchical hexagonal lattice with a stockiness $c/L = 0.091$ and a relative density $\bar{\rho} = 0.05$. The normalized fracture toughness is plotted in Fig. A.1a as a function of the normalized domain width W/L. Recall that W is the width of the square domain (see Fig. 2a) and L is the length of a hierarchical strut. Here, the small-scale struts ℓ were meshed with 10 beam elements at the crack tip. It is clear from Fig. A.1a that the fracture toughness is fairly insensitive to the domain size; predictions vary by less than one percent when W/L is increased from 64 to 128. Based on these results, we selected a size $W/L = 64$ for all our simulations.

A mesh convergence study was then performed (with a domain $W/L = 64$) and the results are plotted in Fig. A.1b. Refining the mesh at the crack tip from 10 to 30 elements per strut ℓ results in a 2% change only in fracture toughness. As a compromise between accuracy and computational efficiency, we decided to use 10 elements per strut in all our simulations.

A.2. Influence of lattice orientation

Additional simulations were conducted to assess the effect the lattice orientation on its fracture toughness. Three orientations, 0°, 15°, and 30°, were considered and these are shown in Fig. A.2 for a hierarchical hexagonal lattice. Note that the 0° orientation is the one considered in this study and it is sufficient to examine rotations up to 30° only because of the six-fold rotational symmetry of each lattice. The effect of orientation for hierarchical hexagonal, triangular, and Kagome lattices with a stockiness of $c/L \approx 0.09$ is shown in Fig. A.3. Clearly,

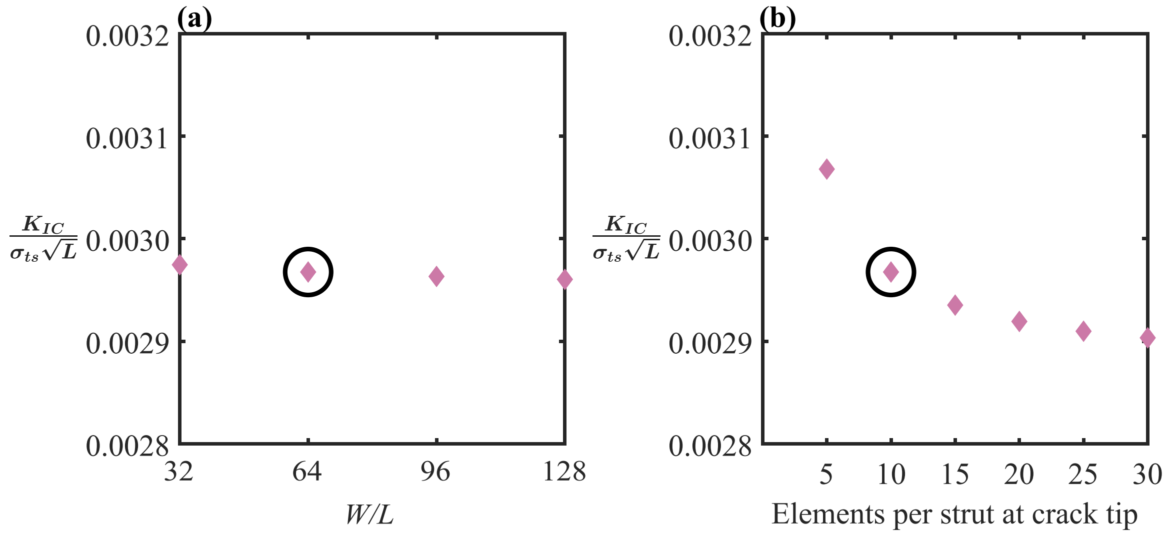

Fig. A.1. Normalized fracture toughness for a hierarchical hexagonal lattice with $\bar{\rho} = 0.05$ and $c/L = 0.091$ as a function of (a) normalized domain width, and (b) mesh size. The domain and mesh sizes employed in all our simulations are circled.

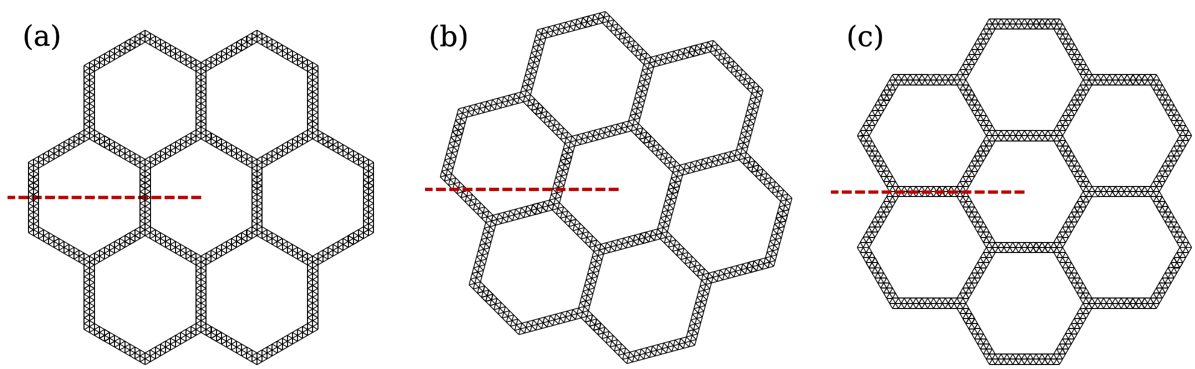

Fig. A.2. A hierarchical hexagonal lattice in the (a) 0°, (b) 15°, and (c) 30° orientations.

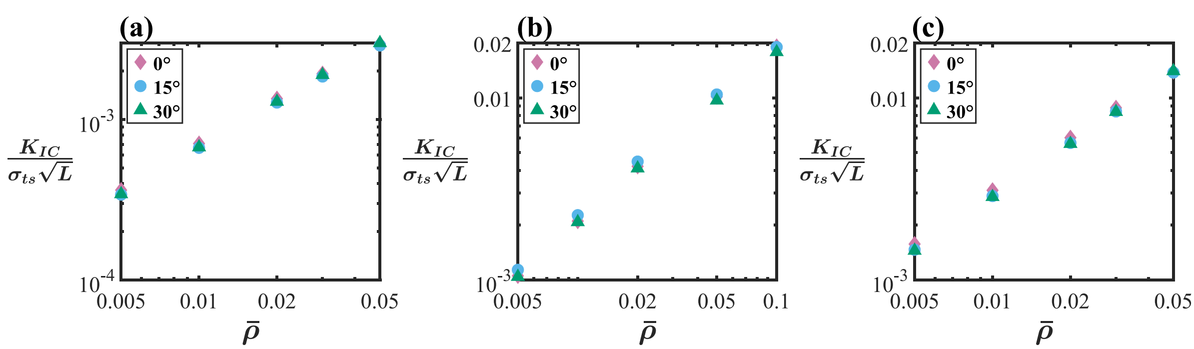

Fig. A.3. Effect of the lattice orientation on the normalized fracture toughness. Results are shown for hierarchical (a) hexagonal, (b) triangular, and (c) Kagome lattices with $c/L \approx 0.09$.

all three hierarchical topologies are fairly insensitive to orientation; the maximum change in fracture toughness is 8% for the range of orientations considered.

A.3. Influence of initial crack path

Cracks propagating in lattices do not break their joints (Lipperman et al., 2007); therefore, cracks are unlikely to be straight like those considered in Fig. 2. To quantify this effect, three alternative, more realistic, initial crack paths were considered, see Fig. A.4. For the hexagonal 30° lattice, the initial crack breaks the inclined bars instead of splitting the horizontal member (compare Figs. A.4a with A.2c). Otherwise, the initial crack paths for triangular and Kagome lattices are modified to avoid going through the joints (compare Figs. A.4b with 2c, and Figs. A.4c with 2d). These additional simulations were performed for lattices with $c/L \approx 0.09$ and $\bar{\rho} = 0.02$. Changing the straight crack to a tortuous path sightly decreased the fracture toughness, with reductions of 0.6%, 1.3% and 1.0% for hexagonal 30°, triangular, and Kagome lattices, respectively. This indicates that the initial crack pattern has a negligible effect on the predicted fracture toughness.

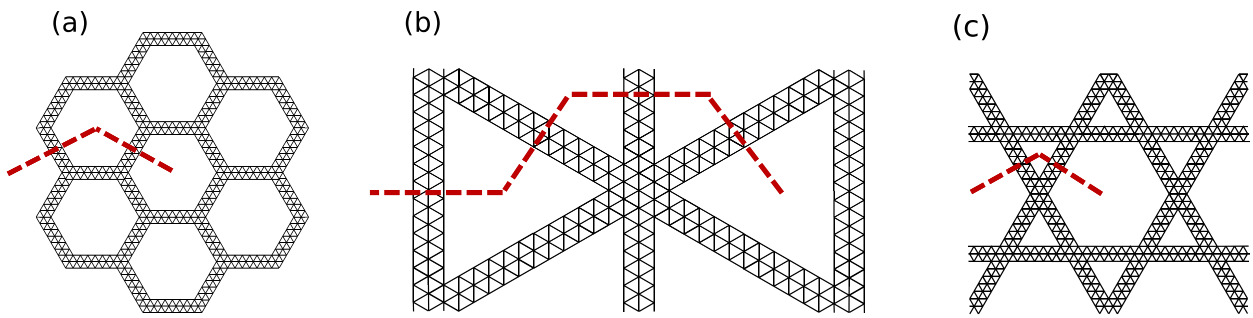

Fig. A.4. Alternative initial crack paths for (a) hexagonal 30°, (b) triangular, and (c) Kagome lattices.

Table B.1
In-plane elastic constants for simple, non-hierarchical lattices.
Source: Data collected from Wang and McDowell (2004).

Topology	B	b	ν
Kagome	1/3	1	1/3
Hexagonal	3/2	3	1
Triangular	1/3	1	1/3

Appendix B. In-plane elastic properties

The in-plane elastic properties of hierarchical lattices are derived analytically in this section. This work relies on the elastic properties of simple, non-hierarchical lattices, which are reviewed below.

B.1. Simple lattices

The elastic modulus of any lattice can be expressed in a non-dimensional form as (Fleck et al., 2010):

$$\frac{E}{E_s} = B\bar{\rho}^b, \tag{B.1}$$

where B and b are topology specific constants given in Table B.1 for simple hexagonal, triangular, and Kagome lattices. Their Poisson's ratio ν is also included in Table B.1. For these three topologies, ν is a function of topology only, and is independent of the parent material.

B.2. Hierarchical lattices

The three hierarchical lattices considered in this work have a six-fold rotational symmetry; therefore, their behavior is transversely isotropic and characterized by two elastic constants: the elastic modulus E and Poisson's ratio ν. Analytical predictions for E are presented below based on the assumption that the behavior of the large-scale lattice is unaffected by introducing hierarchy. Otherwise, we anticipate that simple and hierarchical lattices will have the same Poisson's ratio, and this is also verified below.

A hexagonal lattice is bending-dominated and therefore, its elastic modulus scales linearly with the bending stiffness of the cell walls. Knowing that, and with the values in Table B.1, the elastic modulus of a hierarchical hexagonal lattice can thus be expressed as:

$$E = \frac{3}{2}\bar{\rho}_L^3 \left(\frac{I_h}{I_s}\right) E_s, \tag{B.2}$$

where I_h and I_s are the second moment of area of hierarchical and solid struts, respectively. Keeping only the contribution of the outermost bars, the second moment of area for a hierarchical strut simplifies to:

$$I_h = \frac{tc^2 b_o}{2}, \tag{B.3}$$

Otherwise, for a simple strut of thickness c, we have:

$$I_s = \frac{c^3 b_o}{12}. \tag{B.4}$$

With these two expressions, the ratio I_h/I_s becomes:

$$\frac{I_h}{I_s} = \frac{6t}{c} = \frac{6t}{\sqrt{3}\ell} = \frac{6}{7}\bar{\rho}_\ell, \tag{B.5}$$

where the small-scale relative density $\bar{\rho}_\ell$ was defined earlier in (3). Substituting this in (B.2) and using the definition in (2) and the approximation $\bar{\rho} \approx \bar{\rho}_L\bar{\rho}_\ell$, returns the elastic modulus of a hierarchical hexagonal lattice:

$$\frac{E}{E_s} = \frac{12}{7}\left(\frac{c}{L}\right)^2 \bar{\rho}. \tag{B.6}$$

Simple triangular and Kagome lattices are both stretching-dominated and have the same elastic modulus, see Table B.1. Therefore, the elastic modulus of their hierarchical counterparts can be expressed as:

$$E = \frac{1}{3}\bar{\rho}_L E_s^h, \tag{B.7}$$

where E_s^h is the longitudinal elastic modulus of a hierarchical cell wall. Assuming that the axial load is carried by the three longitudinal bars, E_s^h becomes:

$$E_s^h = \frac{3t}{c}E_s = 0.43\bar{\rho}_\ell E_s, \tag{B.8}$$

which is slightly stiffer than a simple triangular lattice due to size effects (Gu et al., 2018). Substituting (B.8) in (B.7), and using $\bar{\rho} \approx \bar{\rho}_L\bar{\rho}_\ell$, gives the elastic modulus of hierarchical triangular and Kagome lattices:

$$\frac{E}{E_s} = 0.143\bar{\rho}. \tag{B.9}$$

Finite Element simulations were performed to verify these analytical expressions. The in-plane elastic properties were predicted using a single unit cell (see Fig. 1a) with periodic boundary conditions, as described in Markou and St-Pierre (2022). Analytical predictions of the elastic modulus are compared to FE simulations in Fig. B.1 for all three hierarchical designs.

For the hierarchical hexagonal lattice, there is a very good agreement between (B.6) and FE predictions, see Fig. B.1a. Clearly, the elastic modulus of a hierarchical hexagonal lattice scales (i) linearly with relative density (in contrast with its simple counterpart where it scales as $\bar{\rho}^3$) and (ii) with $(c/L)^2$, making stocky configurations much stiffer. There is a small deviation between analytical and FE results when $c/L = 0.19$ because shear and axial deformations of the small-scale lattice become more important, while they are neglected in our analytical modeling.

Our analytical modeling for the hierarchical triangular and Kagome lattices predicts that their elastic modulus should be independent of c/L, see (B.9). Numerical predictions, however, show a slight reduction in E when stockiness c/L decreases, and this is more apparent for the triangular lattice (Fig. B.1b) than the kagome topology (Fig. B.1c). This is attributed to the calculation of relative density: FE simulations are relying on the full expression in (4), whereas our analytical predictions are using $f = 1$ for simplicity. This introduces an error, which increases with c/L and is larger for the hierarchical triangular lattice (since 27 bars are overlapping at the joints instead of 16 in a kagome lattice.).

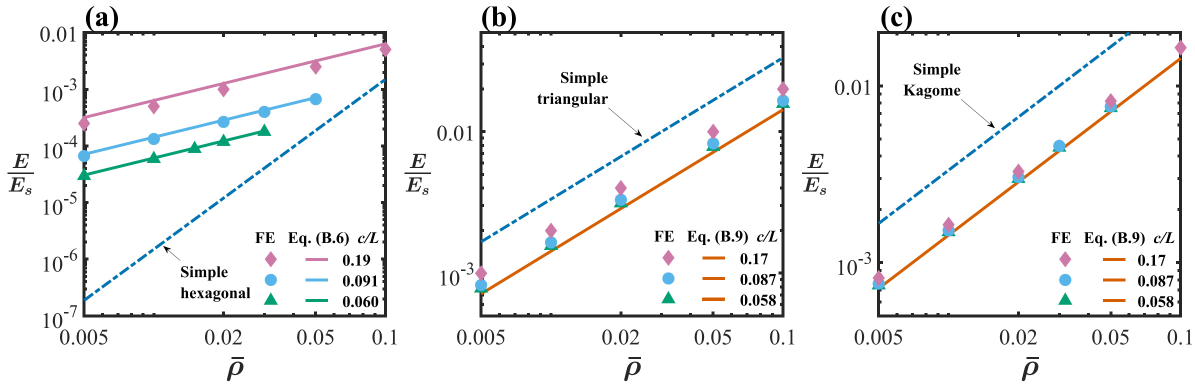

Fig. B.1. Comparison between analytical and FE predictions for the elastic modulus of hierarchical (a) hexagonal, (b) triangular, and (c) Kagome lattices.

Table B.2
Poisson's ratio ν of hierarchical lattices. Results are given for selected values of c/L.

Topology	c/L		
	0.06	0.09	0.18
Hexagonal	0.97	0.94	0.85
Triangular	0.33	0.33	0.33
Kagome	0.33	0.33	0.33

The Poisson's ratio of hierarchical lattices was also obtained from these FE simulations. The values of ν, given in Table B.2, confirm that introducing hierarchy does not affect the Poisson's ratio of the lattice. There is, however, a small reduction in ν with increasing c/L for a hierarchical hexagonal lattice, see Table B.2. This reduction is not a consequence of hierarchy, but instead due to the high stockiness of the cell walls. The same effect has been documented for simple, non-hierarchical hexagonal lattices (Gibson and Ashby, 1997).

Finally, recall that the elastic properties detailed above are necessary as they are part of the displacement field applied to each lattice, see (18). This field, however, is not given as a function of E and ν, but instead expressed with the shear modulus and plane strain Poisson's ratio. Since all topologies are in-plane isotropic, the shear modulus is given by:

$$G = \frac{E}{2(1+\nu)}, \tag{B.10}$$

whereas the plane strain Poisson's ratio is (Romijn and Fleck, 2007):

$$\nu_{ps} = \frac{\nu + B\nu_s^2}{1 - B\nu_s^2}, \tag{B.11}$$

where ν_s is the Poisson's ratio for the parent material, whereas $B = 0.143$ for hierarchical triangular and Kagome lattices, and $B = 12\,(c/L)^2/7$ for hierarchical hexagonal topologies. Note that B is simply the constant of proportionality obtained above in (B.6) and (B.9).

Data availability

Data will be made available on request.

References

Ajdari, A., Jahromi, B.H., Papadopoulos, J., Nayeb-Hashemi, H., Vaziri, A., 2012. Hierarchical honeycombs with tailorable properties. Int. J. Solids Struct. 49 (11), 1413–1419.
Allen, H.G., 1969. Analysis and Design of Structural Sandwich Panels. Pergamon Press.
Berger, J.B., Wadley, H.N.G., McMeeking, R.M., 2017. Mechanical metamaterials at the theoretical limit of isotropic elastic stiffness. Nature 543 (7646), 533–537.
Berkache, K., Phani, S., Ganghoffer, J.-F., 2022. Micropolar effects on the effective elastic properties and elastic fracture toughness of planar lattices. Eur. J. Mech. A Solids 93, 104489.
Côte, F., Russell, B.P., Deshpande, V.S., Fleck, N.A., 2009. The through-thickness compressive strength of a composite sandwich panel with a hierarchical square honeycomb sandwich core. J. Appl. Mech. 76, 061004.
Fleck, N.A., Deshpande, V.S., Ashby, M.F., 2010. Micro-architectured materials: past, present and future. Proc. R. Soc. A 466 (2121), 2495–2516.
Fleck, N.A., Qiu, X., 2007. The damage tolerance of elastic–brittle, two-dimensional isotropic lattices. J. Mech. Phys. Solids 55 (3), 562–588.
Gibson, L.J., Ashby, M.F., 1997. Cellular Solids: Structure and Properties. Cambridge University Press.
Gu, H., Pavier, M., Shterenlikht, A., 2018. Experimental study of modulus, strength and toughness of 2D triangular lattices. Int. J. Solids Struct. 152, 207–216.
Haghpanah, B., Oftadeh, R., Papadopoulos, J., Vaziri, A., 2013. Self-similar hierarchical honeycombs. Proc. R. Soc. A 469, 20130022.
Hedvard, M.L.S., Dias, M.A., Budzik, M.K., 2024. Toughening mechanisms and damage propagation in architected-interfaces. Int. J. Solids Struct. 288, 112600.
Hsieh, M.-T., Deshpande, V.S., Valdevit, L., 2020. A versatile numerical approach for calculating the fracture toughness and R-curves of cellular materials. J. Mech. Phys. Solids 138, 103925.
Hsieh, M.-T., Endo, B., Zhang, Y., Bauer, J., Valdevit, L., 2019. The mechanical response of cellular materials with spinodal topologies. J. Mech. Phys. Solids 125, 401–419.
Kazemahvazi, S., Tanner, D., Zenkert, D., 2009. Corrugated all-composite sandwich structures. Part 2: Failure mechanisms and experimental programme. Compos. Sci. Technol. 69 (7–8), 920–925.
Kooistra, G.W., Deshpande, V.S., Wadley, H.N.G., 2005. Hierarchical corrugated core sandwich panel concepts. J. Appl. Mech. 74 (2), 259–268.
Kostopoulos, V., Vlachos, D., 2017. The buckling response of lattice fuselage structures: validation of finite element models by using smeared unit cell analytical methodology. J. Aeronaut. Aerosp. Eng. 6 (1), 1000185.
Launey, M.E., Ritchie, R.O., 2009. On the fracture toughness of advanced materials. Adv. Mater. 21 (20), 2103–2110.
Lipperman, F., Ryvkin, M., Fuchs, M.B., 2007. Fracture toughness of two-dimensional cellular material with periodic microstructure. Int. J. Fract. 146, 279–290.
Luan, S., Chen, E., Gaitanaros, S., 2022. Energy-based fracture mechanics of brittle lattice materials. J. Mech. Phys. Solids 169, 105093.
Ma, Q., Cheng, H., Jang, K.-I., Luan, H., Hwang, K.-C., Rogers, J.A., Huang, Y., Zhang, Y., 2016. A nonlinear mechanics model of bio-inspired hierarchical lattice materials consisting of horseshoe microstructures. J. Mech. Phys. Solids 90, 179–202.
Maiti, S.K., Ashby, M.F., Gibson, L.J., 1984. Fracture toughness of brittle cellular solids. Scr. Metall. 18 (3), 213–217.
Mangipudi, K.R., Onck, P., 2011. Multiscale modelling of damage and failure in two-dimensional metallic foams. J. Mech. Phys. Solids 59 (7), 1437–1461.
Markou, A., St-Pierre, L., 2022. A novel parameter to tailor the properties of prismatic lattice materials. Int. J. Mech. Sci. 219, 107079.
Omidi, M., St-Pierre, L., 2023a. The fracture toughness of demi-regular lattices. Scr. Mater. 237, 115686.
Omidi, M., St-Pierre, L., 2023b. Fracture toughness of semi-regular lattices. Int. J. Solids Struct. 270, 112233.
Onck, P.R., Van Merkerk, R., De Hosson, J.T.M., Schmidt, I., 2004. Fracture of metal foams: In-situ testing and numerical modeling. Adv. Eng. Mater. 6 (6), 429–431.
Qing, H., Mishnaevsky, Jr., L., 2009. 3D hierarchical computational model of wood as a cellular material with fibril reinforced, heterogeneous multiple layers. Mech. Mater. 41 (9), 1034–1049.
Qing, H., Mishnaevsky, Jr., L., 2011. A 3D multilevel model of damage and strength of wood: Analysis of microstructural effects. Mech. Mater. 43 (9), 487–495.
Romijn, N.E.R., Fleck, N.A., 2007. The fracture toughness of planar lattices: Imperfection sensitivity. J. Mech. Phys. Solids 55 (12), 2538–2564.
Ryvkin, M., Shraga, R., 2018. Fracture toughness of hierarchical self-similar honeycombs. Int. J. Solids Struct. 152, 151–160.

Schmidt, I., Fleck, N.A., 2001. Ductile fracture of two-dimensional cellular structures. Int. J. Fract. 111, 327–342.

Seiler, P.E., Tankasala, H.C., Fleck, N.A., 2019. The role of defects in dictating the strength of brittle honeycombs made by rapid prototyping. Acta Mater. 171, 190–200.

Shaikeea, A.J.D., Cui, H., O'Masta, M., Zheng, X.R., Deshpande, V.S., 2022. The toughness of mechanical metamaterials. Nat. Mater. 21 (3), 297–304.

Sun, F., Lai, C., Fan, H., Fang, D., 2016. Crushing mechanism of hierarchical lattice structure. Mech. Mater. 97, 164–183.

Tancogne-Dejean, T., Diamantopoulou, M., Gorji, M.B., Bonatti, C., Mohr, D., 2018. 3D plate-lattices: an emerging class of low-density metamaterial exhibiting optimal isotropic stiffness. Adv. Mater. 30 (45), 1803334.

Tankasala, H.C., Deshpande, V.S., Fleck, N.A., 2015. 2013 Koiter medal paper: crack-tip fields and toughness of two-dimensional elastoplastic lattices. J. Appl. Mech. 82 (9), 091004.

Tankasala, H.C., Fleck, N.A., 2020. The crack growth resistance of an elastoplastic lattice. Int. J. Solids Struct. 188, 233–243.

Taylor, C.M., Smith, C.W., Miller, W., Evans, K., 2011. The effects of hierarchy on the in-plane elastic properties of honeycombs. Int. J. Solids Struct. 48 (9), 1330–1339.

Torquato, S., Gibiansky, L.V., Silva, M.J., Gibson, L.J., 1998. Effective mechanical and transport properties of cellular solids. Int. J. Mech. Sci. 40 (1), 71–82.

Tran, T., Hou, S., Han, X., Tan, W., Nguyen, N., 2014. Theoretical prediction and crashworthiness optimization of multi-cell triangular tubes. Thin-Walled Struct. 82, 183–195.

Vigliotti, A., Pasini, D., 2013. Mechanical properties of hierarchical lattices. Mech. Mater. 62, 32–43.

Wang, A.-J., McDowell, D., 2004. In-plane stiffness and yield strength of periodic metal honeycombs. J. Eng. Mater. Technol. 126 (2), 137–156.

Wang, P., Yang, F., Zheng, B., Li, P., Wang, R., Li, Y., Fan, H., Li, X., 2023. Breaking the tradeoffs between different mechanical properties in bioinspired hierarchical lattice metamaterials. Adv. Funct. Mater. 33 (45), 2305978.

Yang, X., Zhang, B., 2024. Fracture of four semi-regular lattices regulated by T-stress in modified boundary layer models. Mech. Mater. 195, 105026.

Yin, S., Chen, H., Li, J., Yu, T., Xu, J., 2019. Effects of architecture level on mechanical properties of hierarchical lattice materials. Int. J. Mech. Sci. 157, 282–292.